NASA TM- 81271

NASA Technical Memorandum 81271

Flight Investigation of a Four-Dimensional Terminal Area Guidance System for STOL Aircraft

Frank Neuman and Gordon Hardy

March 1981

National Aeronautics and
Space Administration

NASA Technical Memorandum 81271

Flight Investigation of a Four-Dimensional Terminal Area Guidance System for STOL Aircraft

Frank Neuman
Gordon Hardy, Ames Research Center, Moffett Field, California

National Aeronautics and
Space Administration

Ames Research Center
Moffett Field, California 94035

FLIGHT INVESTIGATION OF A FOUR-DIMENSIONAL TERMINAL AREA GUIDANCE SYSTEM FOR STOL AIRCRAFT

Frank Neuman and Gordon Hardy

Ames Research Center

SUMMARY

A series of flight tests and fast-time simulations have been conducted, using the augmentor wing jet STOL research aircraft and the STOLAND 4D-RNAV system to add to the growing data base of 4D-RNAV system performance capabilities. To obtain statistically meaningful data a limited amount of flight data were supplemented by a statistically significant amount of data obtained from fast-time simulation. In this paper, the results of these tests are reported. Included are comparisons of the 4D-RNAV estimated winds with actual winds encountered in flight, as well as data on along-track navigation and guidance errors, and time-of-arrival errors at the final approach waypoint. In addition, an improvement of the STOLAND 4D-RNAV system is proposed and demonstrated, using the fast-time simulation.

INTRODUCTION

Traffic capacity within the air traffic control system can be increased by closer spacing and more precise sequencing of aircraft, especially in the terminal area (ref. 1). To achieve such precision, a concept of precise control of the aircraft in both position and time, referred to as 4D-RNAV, has been proposed (ref. 2) and shown to be effective (refs. 3-5). Preliminary system analysis and simulation studies considered path changing (ref. 6) and speed control (ref. 7) or both (ref. 8) to achieve controlled time of arrival. Early studies considered an ideal environment with no navigation errors and winds that were known. In recent years several other analytical and simulation studies of improved 4D-RNAV systems that considered environmental disturbances have been published (refs. 9-15).

To study detailed problems of 4D-RNAV in a real environment, such systems must be implemented and flight tested. Two different flight-director 4D-RNAV systems have been test flown in a Convair 340 to simulate slow STOL steep approaches (5°). Both systems used preselected *airspeed* profiles and wind estimates to control time of arrival (refs. 16-18). It was shown that the desired time of arrival could be met within ±3 sec (2σ); moreover, the navigation system permitted smooth transition from area navigation to precision terminal navigation with an acceptable pilot rating for the overall guidance task. Automatic and flight-director 4D-RNAV flight tests, using a conventional jet transport plane, have been reported in reference 19. Time control

was maintained by flying a preselected *groundspeed* profile along the reference path, regardless of winds.

The purpose of this paper is to add to this growing data base of 4D-RNAV systems by reporting the performance of the 4D-RNAV system installed in the Augmentor Wing Jet STOL Research Aircraft (AWJSRA). To obtain meaningful statistical data, a procedure (borrowed from certification of automatic landings) was used in which a limited number of flight tests are conducted to verify the performance of the system, and a fast-time Monte Carlo simulation study is conducted to provide meaningful statistical data. In this paper the results of both the flight tests and fast-time simulation studies are presented and compared. This is followed by the results of a fast-time simulation study directed at verifying a proposed improvement in the 4D-RNAV algorithm.

The AWJSRA is a two-engine turbofan aircraft with swiveled hot-gas exhaust nozzles and with the cold flow from the front fans ducted to augmented jet flaps (ref. 20). The aircraft is equipped with an integrated digital avionics system (STOLAND, ref. 21) which includes a computer that can handle all navigation, guidance, and control computations. The flight-test facility included a TACAN station, a microwave landing system, and an extensive tracking radar and data acquisition facility.

EXPERIMENTAL EQUIPMENT FACILITIES AND SIMULATIONS

The experimental equipment used in this study includes the AWJSRA, a real-time fixed-base simulation facility, and a fast-time 4D-RNAV simulation facility.

Augmentor Wing Jet STOL Research Aircraft Description

The AWJSRA is a modified deHavilland C-8A "Buffalo." Its wing area, S, is 80.36 m^2 (865 ft^2) and its maximum gross weight is 21,772 kg (48,000 lb). The aircraft is powered by two turbofan engines.

The cold flow from the engine fans is ducted through the wing and fuselage to the augmentor jet flap and blown ailerons. The augmentor flap pivots about the flap hinge point. No provision is made in this installation to retract the flap into the main wing contour. The Coanda surface serves to deflect the (cold) flow from the nozzle. The chokes at the trailing edges of the main flaps control the lift generated by the flaps. Two outboard chokes are used for roll control and two inboard chokes are used for direct lift control during the final approach.

The hot gas from the two engines flows through two pairs of nozzles; the nozzles can be rotated through 98° in flight to provide vectoring of the hot thrust. In automatic flight, the nozzles respond in unison to a single nozzle-angle command. The servos that control the nozzles are rate limited

at 90°/sec. In automatic flight the speed of both engines is controlled in unison by a single throttle command. The associated throttle servo system is relatively slow, with a bandwidth of approximately 1 rad/sec.

The cold flow has a pronounced effect on the lift-drag polars of the aircraft. There is a substantial change between the cruise configuration (5.6° flap) and landing configuration (6.5° flap). Automatic trajectory tracking systems have to cope with the large variation in the lift-draft characteristics of such aircraft.

Flight-Test Facility

The flight data were obtained at the Naval Auxiliary Landing Field (NALF) Crows Landing Test Facility. The facility includes a simulated STOL runway, which is 591 m (1939 ft) long, a TACAN station for terminal-area navigation, and an experimental microwave landing system, MODILS (ref. 8). It also includes a tracking radar to provide position and velocity data for postflight calculation of navigation errors. The tracking data were smoothed with a minimum mean square second-order curve fit over ±3 sec to obtain a best estimate of the actual aircraft position.

A radio downlink transmits all sensor data from the aircraft to a display and computational facility. At this facility, the downlinked data and the tracking radar data are time correlated, merged, and recorded, using a digital computer. Thirty-two channels of data can be selected and displayed in real time on a strip-chart recorder and monitored by the test engineer. A display is also presented to the test engineer on a TV monitor, which duplicates the information on the mode-select panel in the aircraft. Voice communication with the aircraft is maintained at all times.

Real-Time Simulation

Ames Research Center operates an extensive real-time simulation facility. This facility includes flight hardware, permits preflight testing of all aircraft system modes. It is used to: (1) develop systems concepts, (2) establish a data base for each concept to be validated by flight tests, (3) validate software prior to flight, (4) train pilots, and (5) reduce and interpret data postflight.

The link between the simulator and flight hardware is the airborne hardware simulator (AHS). The AHS converts digital sensor simulation signals from the simulation computer (EAI 8400) to the formats of the airborne sensors and NAVAID receivers. These signals are then fed into the flight hardware mounted in the equipment rack, which, in turn, interface with the displays and control panels in the simulation cockpit.

Fast-Time 4D-RNAV Simulation

Several simplifying assumptions were made in order to produce a fast-time simulation with which to study RNAV system performance. First, the lateral and vertical control systems were not simulated. This is equivalent to assuming that the actual systems are able to maintain the aircraft on the indicated reference path independent of winds or path distortions caused by navigation errors. Second, the dynamics of the speed control system were represented by a low-pass filter with a 3-sec time constant between commanded and calibrated airspeed. Third, it was assumed that filtering would not reduce the very slowly changing position errors that result from time-invariant bias errors in the navigation aids. Thus, the complementary navigation filters were not simulated. Also, the change in bias-error effects on position estimation with altitude have been neglected, thus reducing the problem from one of three dimensions to one of two dimensions. When NAVAID bias errors were simulated, the groundspeed measurement error caused by the bias errors was added to the wind velocity and filtered with an 80-sec low-pass filter to represent the estimated winds. Comparison with real-time simulation data showed these to be reasonable assumptions (appendix A).

To provide a realistic wind profile, 27 sample wind profiles were used. These sample profiles were observed and recorded at 305-m (1000-ft) altitude intervals at the Oakland, Calif., weather station. From these sample profiles a wind model was also developed from which an infinite number of wind profiles could be generated (appendix A). For some studies, a random wind component was added to a chosen average wind profile. The random wind was generated by filtering wideband Gaussian pseudorandom noise through a $\tau = 900$ sec time constant low-pass filter of proper gain to produce a desired random wind standard deviation.

AVIONICS SYSTEM DESCRIPTION

The AWJSRA is equipped with STOLAND, an integrated digital avionics system. The system is programmed to perform all terminal-area navigation, guidance, and automatic control functions along a curved reference approach flightpath. Included in the system are the autopilot modes, considered standard for commercial transport aircraft, and an autothrottle. The major components of the system are a Sperry 1819A general-purpose digital computer and a data adapter that interfaces all the navigation aids, displays, controls, and servo actuators with the computer. The navigation aids include VHF omnirange (VOR), distance measuring equipment (DME), tactical air navigation (TACAN), a microwave modular instrument landing system (described in ref. 8 (MODILS)), and a radio altimeter.

System components installed in the cockpit of the aircraft include a horizontal situation indicator (HSI), an electronic attitude director indicator (EADI), a multifunction display (MFD) and MFD control panel, a mode-select panel (MSP), a status panel, and a data-entry panel. During automatic operation, the pilot monitors the system operation through the various cockpit

displays. During flight-director operation, the pilot uses the same set of displays to fly the aircraft along the reference flightpath and to monitor the system. A detailed description of the system operation is given in reference 7.

The Navigation System

The navigation system provides estimates of the aircraft position and velocity with respect to a runway coordinate system which has its origin at the glide-slope intercept point (fig. 1). The position and velocity estimates are generated using ground-navigation-aid information blended in a complementary filter with inertial information obtained from body-mounted accelerometers and attitude sensors, magnetic heading, barometric altitude, and true airspeed.

The ground navigation data are obtained from TACAN, except when the aircraft is in MODILS coverage after passing point A (fig. 1). The navigation system also estimates wind velocity. In the event of a momentary loss of ground-radio-navigation-aid information, navigation is accomplished by dead reckoning, using air data and inertial data. Upon regaining radio information, the system automatically switches back to the use of radio data. A detailed description of the navigation system is presented in reference 9. Subsequent changes made to that system are described in appendix D.

The Guidance System

4D-RNAV path specification- The guidance system used during the landing approach is based on a flightpath stored in the airborne computer. The flightpath is specified by waypoints (X, Y, Z coordinates) and associated information, such as the radius of turn between waypoints and the maximum, minimum, and nominal airspeed between waypoints V_{max}, V_{min}, and V_{nom}. An illustration of an approach flightpath in the AWJSRA is shown in figure 1. It consists of a long inbound leg (waypoints 1-9); a 180° turn to final approach (waypoints 9, 10), with a 7.5° glide slope occurring after the turn (waypoint 11); and a final straight-in approach (waypoints 11, 12). The guidance system is essentially independent of the type of aircraft and independent of whether the system is manual or automatic. The guidance laws are separated into lateral tracking, vertical tracking, and speed control for time of arrival. A detailed description of the system is given in appendix A of reference 3. The AWJSRA's speed/safety limits are described in appendix C.

Time-of-arrival guidance system- The object of time-of-arrival guidance is to permit the aircraft to arrive at a specified waypoint within a closely defined time interval, in order to permit high-density sequencing operations for aircraft in the terminal area. The time-of-arrival guidance at the final waypoint is based on speed control only. Path stretching capability has not been provided.

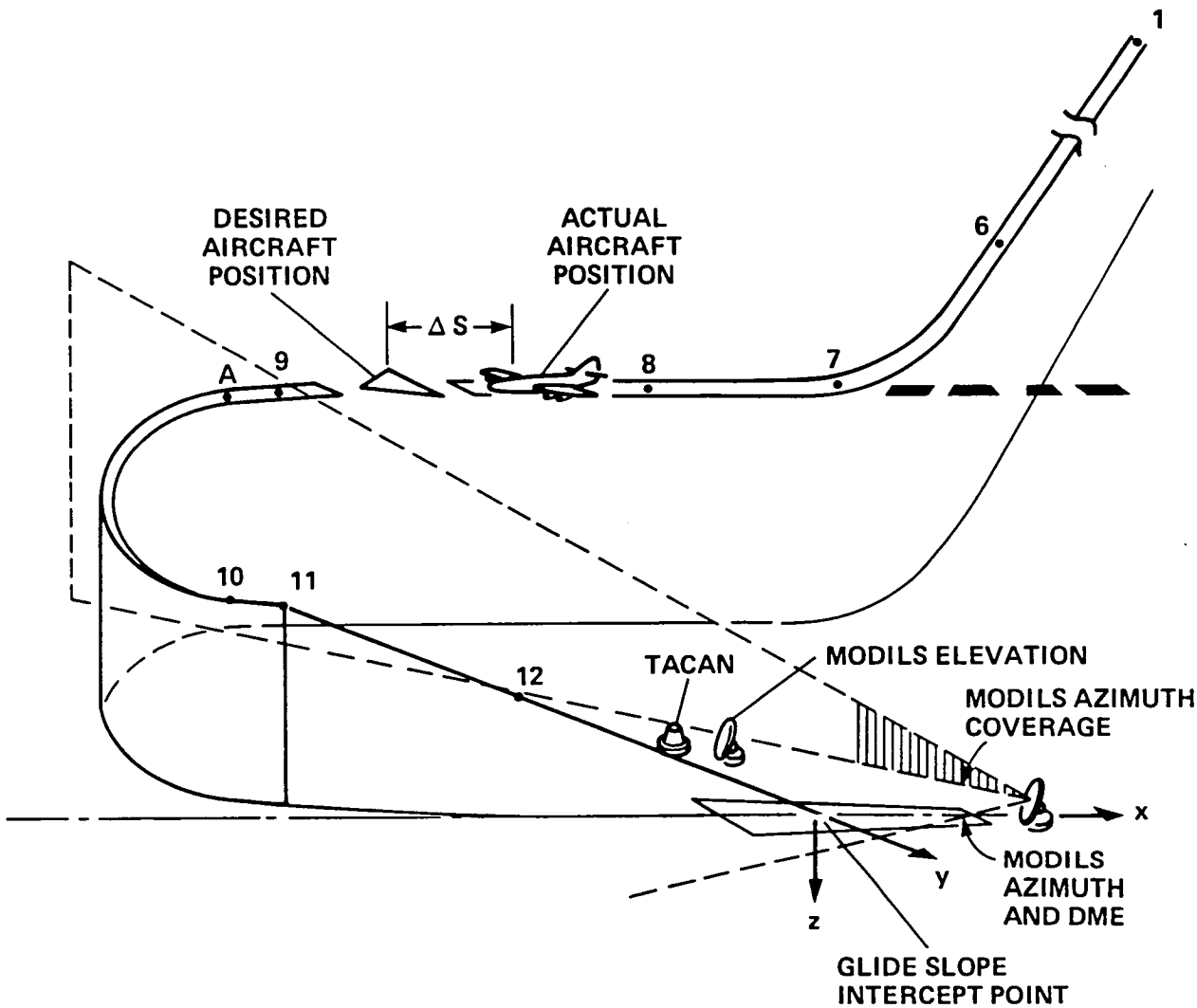

Figure 1.- Approach flightpath.

Speed control for 4D-RNAV is achieved by providing an airspeed command to the aircraft speed control system. The airspeed command, V_c, is defined to be the sum of a prescribed nominal airspeed V_{nom} and an error that is proportional to an aircraft position error, ΔS, illustrated in figure 1

$$V_c = V_{nom} + K_f \Delta S \left|\frac{T_{ref}}{T}\right|_{\leq 1}$$

where $K_f = 0.04$ sec, T = time-to-go, and T_{ref} = time-to-go at which maximum constant gain is used. The term ΔS is the distance along the track from the aircraft position to a moving desired position, which is positive when the desired position is ahead of the aircraft. The last factor, $|T_{ref}/T|_{\leq 1}$ is used to prevent a large deviation of V_c from the nominal speed when the aircraft is far from the final position. The commanded airspeed V_c is also governed to fall between specified speed limits that are dictated by aircraft structural design safety margins and ATC considerations.

Initially, at the aircraft's arrival at the first selected waypoint, the aircraft's desired and actual positions coincide. Two techniques were used to compute the time it will take from the selected capture waypoint to the final waypoint. The original technique referred to herein as the "constant-wind technique" is based on the assumption that the wind will remain at its current estimated value throughout the remainder of the approach. It was found, as will be shown, that this results in large time-of-arrival errors. The technique was then modified to assume that the wind changes linearly from its current estimate to the ground-measured wind at the final waypoint. The ground wind would be manually inserted by the pilot. The latter technique, referred to as the "variable-wind technique," was not evaluated in flight but was evaluated in both the real- and fast-time simulations. From the foregoing discussion it is apparent that with either technique the nominal time of arrival will not be known until passing the first waypoint, nor can it be preassigned. In an operational system, this would not fulfill the requirements. One solution, investigated at Ames Research Center, employs a continuously recomputed capture flightpath to a selected waypoint to achieve the desired time of arrival (ref. 17).

With both techniques the desired position of the aircraft is recomputed every 10 sec, based on the latest estimate of wind velocity and direction, such that the final waypoint arrival time will be satisfied with the least deviation from the nominal airspeed V_{nom}. As long as the aircraft and the desired target position coincide, the aircraft will only deviate from nominal airspeed if there are changes in the estimated wind velocity or if navigation errors occur. Details of the calculations are given in reference 16.

The Automatic Control System

Overview- To achieve time-of-arrival guidance, the AWJSRA has two automatic modes of operation: the cruise mode and the STOL mode. In the cruise mode the primary vertical force on the aircraft is due to the lift from the

wings, and the primary horizontal force is due to thrust from the engines and the drag of the aircraft configuration. Therefore, it is natural to control vertical flightpath with pitch and to control speed with throttle. The nozzle angles are held constant at 6°. The vertical-path-control law generates a pitch command, which controls the elevator via a pitch-control stabilization feedback loop. The autothrottle-control law generates a throttle rate command to stabilize the system. A trimtable, which is part of the control system, reduces the amount of error correction the control laws have to accomplish when reference values, such as flightpath angle or airspeed, change. As inputs, the table uses (1) reference flightpath angle, (2) flap angle, (3) nozzle angle, and (4) airspeed. The outputs of the table are reference throttle and pitch commands.

As the speed decreases on final approach and the flap setting is greater than 45° the STOL mode of operation is engaged automatically. In the STOL mode, flaps and nozzles are deployed to allow steep approaches, and the aircraft is operated on the backside of the power curve. Hence, pitch is chosen for speed control and throttle for flightpath control.

In the automatic 4D-RNAV mode, the flaps deploy automatically during 4D deceleration segments, and the nozzles deploy for some descending approach configurations with the flaps down. This automatic control of the flaps and nozzles is described below in more detail.

Configuration control: automatic flap control- To minimize workload in manual operation, pilots increase flap settings incrementally. The automatic system can control flaps in a continuous manner. Automatic continuous control can make the approach more fuel-efficient, particularly if the flaps are deployed as late as possible. Automatic flap control is a vital part of automatic configuration control for powered-lift STOL aircraft since it decreases pilot workload and permits the pilot to spend more time monitoring overall system performance.

Before deploying the flaps automatically, the flap control system requires that (1) the flap servo be selected, and (2) that the pitch control system be functioning. When these conditions are satisfied, the system compares the reference airspeed with the minimum airspeed allowable for the present aircraft configuration, IAS_{min} (see appendix D). If the command airspeed V_c is greater than the minimum airspeed $V_{c_{min}}$, the flap position remains unchanged. If V_c corresponds to $IAS_{com} < IAS_{min}$, the flaps are deployed at a rate that is somewhat less than 2°/sec until $IAS_{com} = IAS_{min}$. Because of safety considerations, the automatic system is permitted to lower the flaps but not retract them, even though the 4D-RNAV may require an increase in speed to make up for time errors.

When the aircraft is on the final part of glide-slope tracking, it must be brought quickly to the full-flap landing configuration. For this purpose a flap waypoint is defined, past which the flaps are deployed at the maximum possible rate without exceeding the flap placard speeds.

Configuration control: automatic nozzle control- In the cruise configuration, the aircraft nozzles are held in the up position (6°). The nozzles are deployed automatically if (1) the flaps are down more than 45° or if the MLS glide slope is captured and (2) a descending flightpath angle steeper than or equal to 4° is being commanded.

The nozzle deployment rate is 20°/sec and the final position is a function of the aerodynamic flightpath angle required to achieve the inertial flightpath angle commanded. This aerodynamic flightpath angle is calculated as the ratio of groundspeed to true airspeed multiplied by the inertial flightpath angle. The result is that the nozzle angle varies with wind speed for a given speed and inertial descent angle. The net effect is to trim the configuration of the aircraft so that the trimmed engine rpm settings remain in the region of 93-95% N_H, irrespective of the inertial flightpath and winds on a standard day. When the aircraft is turning, the nozzles are raised slightly to allow the power setting to remain constant in the turn.

The overall nozzle command is limited to less than 104° for altitudes above 70 m (200 ft). To prevent debris ingestion, below 70 m (200 ft) above the runway this limit changes to 90°. If the nozzles are more than 90° at 70 m (200 ft) they are driven back to 90° at a rate of 10°/sec. In addition, below 18.29 m (60 ft) the nozzle command will remain at the value it had at 18.29 m (60 ft).

Illustration of automatic configuration control system operation- The operation of the automatic configuration control system will be illustrated by discussing the data for a representative approach, which are shown in figure 2. The dash-dot line in figure 2(a) is the nominal speed V_{nom}, and the dashed lines labeled V_{max} and V_{min} represent the minimum and maximum speeds that the 4D-RNAV system can command, irrespective of the aircraft configuration or control mode. The difference between maximum and minimum speeds allows for time-of-arrival control. It can be seen that most of the terminal path consists of deceleration segments. In the last flight segment (waypoints 11, 12) the speed envelope converges to the aircraft's landing airspeed, and this converging speed envelope reduces the speed difference available for time-of-arrival control for the final portion of the flight.

The heavy solid line in figure 2(a) is the actual speed command IAS_{com} that corresponds to the desired V_c for a typical flight; IAS_{com} is sometimes above and sometimes below the 4D nominal speed in an attempt to meet the nominal time of arrival as winds and navigation errors change. Although V_{nom} is true airspeed, the differences between indicated and true airspeed were negligible for these flights. Figure 2(a) also shows (dotted lines) the aircraft configuration-dependent safety limits, IAS_{max} and IAS_{min}, which are superimposed on the 4D command speed. As shown in figure 2(b) the flaps begin to be deployed when the command speed IAS_{com} goes below IAS_{min}, which is the airspeed that guarantees a maneuver margin of 0.69 g. Since, to save fuel, the flap is deployed to the minimum angle which guarantees the specified maneuver margin, IAS_{min} and IAS_{com} coincide during flap deployment. If, however, at $t = 100$ sec, the 4D system had suddenly required a speed increase of 20 knots to V_{max}, IAS_{com} would have increased only by 10 knots to IAS_{max}

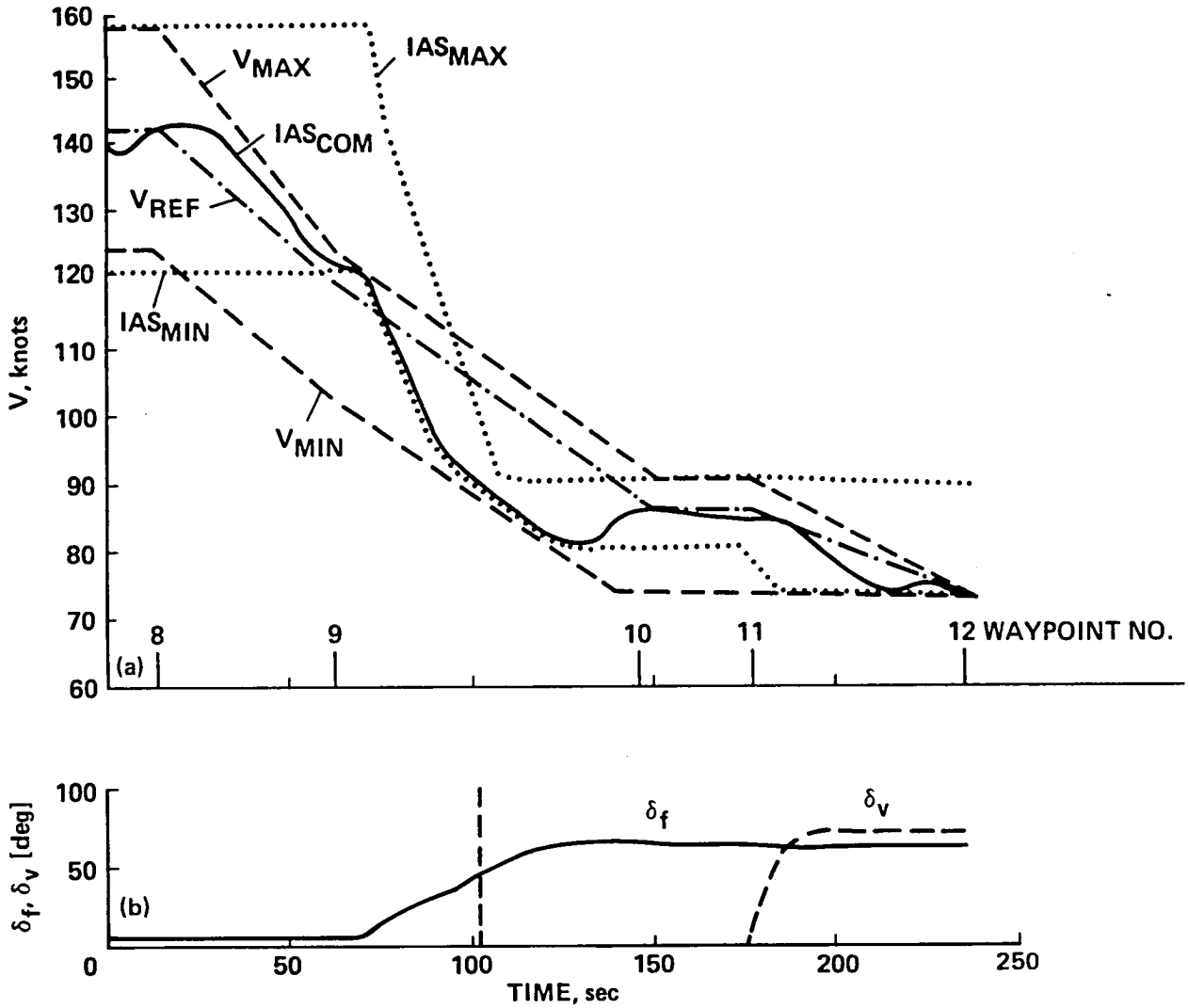

(a) Reference speeds.

V_{REF} —·— 4D REFERENCE SPEED. A/C WOULD FLY THIS SPEED IF NO ERRORS OCCUR

V_{MAX} – – – } 4D SYSTEM CAN COMMAND THIS RANGE OF SPEEDS TO CORRECT FOR
V_{MIN} – – – } ERRORS INDEPENDENT OF AIRCRAFT CONFIGURATION

IAS_{MAX} ····· FLAP PLACARD SPEED LIMIT } = $f(\delta_f, \delta_\nu)$
IAS_{MIN} ····· MANEUVER MARGIN LIMIT }

IAS_{COM} ——— AIRSPEED COMMAND AFTER BOTH 4D RNAV AND SAFETY LIMITS ARE APPLIED TO THE 4D RNAV SPEED COMMAND

(b) Configuration control: flaps δ_f and nozzle δ_v.

Fig. 2.- TOA control.

(since flap retraction was forbidden in these tests), and the flaps would have remained fixed until the speed command again would go below 90 knots.

As discussed in the preceding subsection, the nozzle is deployed as a function of the commanded glide-slope angle. The nozzle angle δ_ν which shows little variation for different approaches is shown in figure 2(b). As the trace for IAS_{min} shows, only after the nozzle is fully deployed is a speed command as low as the landing airspeed permitted. This configuration control can limit the authority of the 4D system and thus contribute to time-of-arrival errors.

TEST PROCEDURES

The performance of the time-of-arrival control system has been determined both in flight and in the fast-time simulation for the reference flightpaths shown in figure 3. The flight tests were initiated at an altitude of 1329 m (4360 ft) to determine the system performance in winds which varied with altitude. The flightpath was designed to minimize flight time while providing a complex path. The fast-time simulator flights were initiated at an altitude of 2408 m (7900 ft) to study effects of winds with larger altitude changes.

Flight Test

The flight test was conducted to check for problems arising from component errors, such as sensor errors, that cannot be considered in the simulations, and to validate the simulation data. The data recorded during the flight test included: (1) the winds encountered and the 4D-RNAV estimated winds, in order to determine how well the 4D-RNAV system was able to estimate the winds; (2) the TACAN and MLS bearing and distance errors, to aid in understanding the navigational environment in which the tests were conducted; (3) the along-track navigational errors, to aid in understanding their effect on time-of-arrival errors; (4) the along-track guidance errors, to aid in understanding their effect on time-of-arrival errors; and (5) the time-of-arrival errors, which are the primary measure of the 4D-RNAV system performance.

Because of operating costs, only the constant-wind 4D-RNAV technique was evaluated in flight. Two approaches were made along the complete flightpath, starting at waypoint 1, and 10 approaches were made starting at waypoint 7 (to conserve flight time). The 12 approaches were flown on three different days (the flights are referred to here as flights 1, 2, and 3, respectively). In addition to these 12 approaches, 5 other approaches, starting from waypoint 1, were flown over most of the approach; however, for various reasons they were aborted prior to reaching waypoint 12.

Three methods were used to check on-board wind measurements. First, balloons were launched and tracked by radar to obtain wind magnitude and direction versus altitude over the test site. Second, a ground-wind measurement station, which records wind magnitude and direction, was installed at

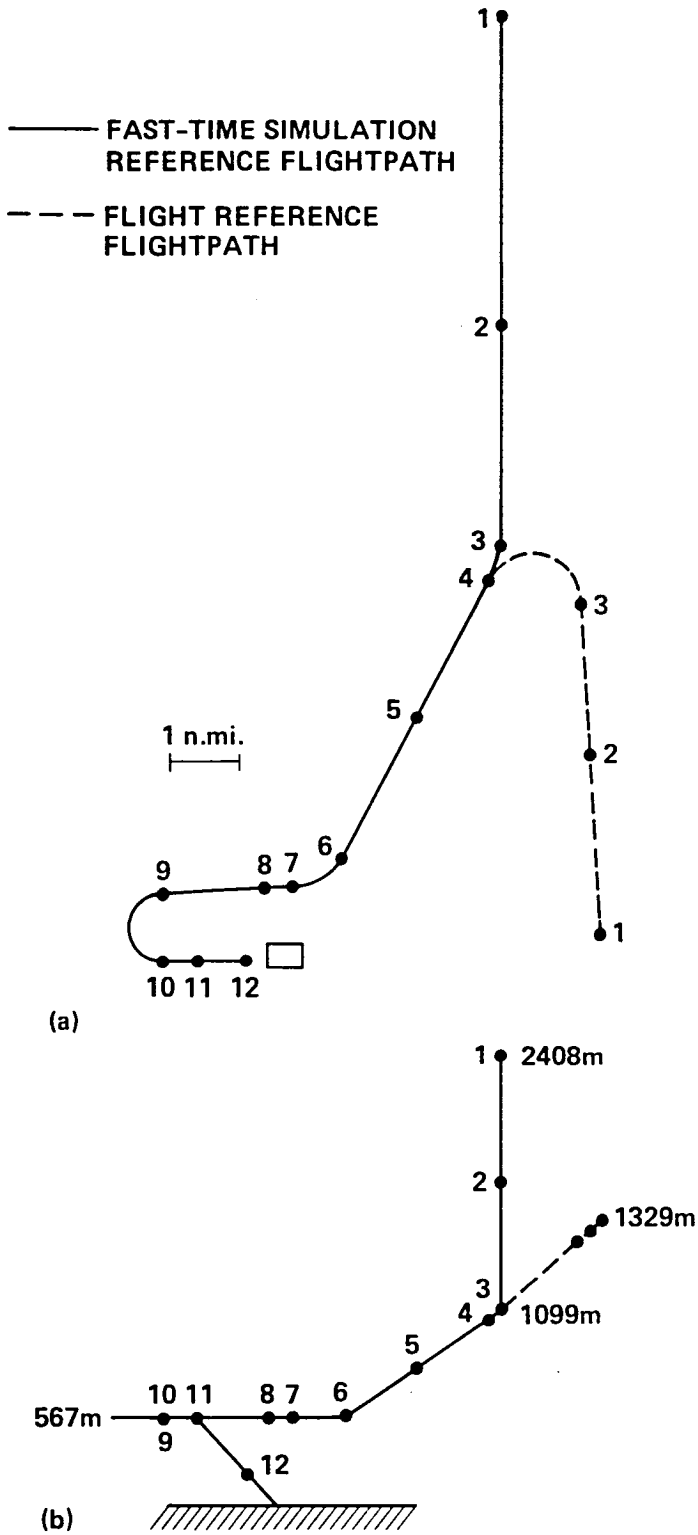

Figure 3.- Reference flightpath.

the STOL runway threshold. Third, the best available estimate of the wind at the aircraft was obtained by using tracking radar combined with air data. The air data and radar were smoothed via a minimum mean squared error algorithm.

Real-Time Simulation

The real-time simulation was used to develop and check out the flight digital computer program and for pilot familiarization. In addition, it was used to verify the fast-time simulation (see appendix A).

Fast-Time Simulation

The fast-time simulation was used as a base for an intuitive understanding of the system's operation and to obtain the statistical performance of the system. For each simulated flight a wind profile was randomly chosen from the wind model described in appendix E, and navigation bias errors were selected from the navigation bias error model described in appendix F.

Four statistical quantities (tabulated for all tests in appendix D) were used to characterize each simulated flight. First, the average of the absolute value of the difference between command and nominal velocity $|V_c - V_{nom}|$ was used to indicate the tracking error from the nominal speed profile. Second, the standard deviation of the change in speed command over a given time interval, $(\Delta V_c/\Delta t)$ was used as a measure of throttle activity. Third, the average of the absolute value of the position error between the aircraft actual and desired position, $\overline{|\Delta S|}$, was used as a measure of the strictness of speed control. Fourth, the time-of-arrival error T_e, which is the difference between predicted and actual time of arrival, was used as the primary measure of the overall system performance.

The number of times the speed command was limited, either because of 4D-RNAV-specified limits or because of aircraft maneuver margin or flap placard limits, was also recorded. For specific runs in which more complete output was desired, 24 channels of analog data were recorded and pertinent statistical data accumulated.

Both 4D-RNAV techniques were evaluated on the fast-time simulation. For the constant-wind technique, in which the winds measured at the aircraft were assumed to be constant over the remaining portion of the flightpath, 770 simulated flights were made along the entire flightpath (fig. 3); in addition, 2000 simulated flights were made which began at waypoint 7. Results of these tests, as well as many others, are given in appendix B.

To study the variable-wind 4D-RNAV technique, in which the wind was assumed to change linearly with altitude, from the wind measured at the aircraft to the wind measured at the airport, 170 pairs of simulated flights were made with winds selected from the wind-profile model described in appendix A but without navigation errors. To investigate the effect of both

navigation errors and wind profiles on the time-of-arrival calculation, an additional 365 simulated flights were made, using the navigation error models described in appendix F and the wind models described in appendix E.

RESULTS AND DISCUSSION

Flight Test

Wind estimates- Because the performance of the 4D-RNAV guidance system is affected by how well the system estimates the winds, the winds derived by the 4D-RNAV system are compared in figure 4 with the winds determined from radar/air-data measurements (light solid lines) and the balloon measured winds (dashed lines). The balloon wind measurements were taken either before or after each flight. As seen in figure 4, the balloon-measured winds agree quite well with the radar/air-data derived winds; they are interpreted as being a reasonable approximation of the actual winds.

The 4D-RNAV estimated winds are obtained by blending TACAN or MLS measurements with air data and magnetic heading. The accuracy of the navigation aids therefore has a significant effect on the wind estimate. This is evident in figure 4 which shows the large errors in the on-board derived wind estimates between waypoints 1 and 9 where TACAN is the primary navigation aid. Once the aircraft gets into the MLS coverage (waypoints 10-12) these errors are significantly reduced. The large errors in the wind estimates between waypoints 1 and 9 can be expected to affect the time-of-arrival errors at waypoint 12.

Navigation and guidance errors- For the TACAN, the standard deviation of the high-frequency noise in the bearing signal was about 0.17°. The superimposed bias error for Flight 1 was 0°, for Flight 2 it was 0.15°, and for Flight 3 it was about 0.2°. For the other five long approaches, the TACAN bias error was about 1°. For the TACAN DME, the standard deviation of the high-frequency noise for all flights was 38 m (125 ft). The bias error was +69 m (226 ft) for Flight 1, -61 m (200 ft) for Flight 2, and -84 m (276 ft) for Flight 3. For the other five long approaches it was between -90 m (295 ft) and 180 m (590 ft).

For the MODILS, the standard deviation of the high-frequency noise in the azimuth was 0.083°. The bias error for all flights was a constant 0.13°. These values held for all 12 approaches. For the MODILS DME, the standard deviation of the high-frequency noise was 8.9 m (29 ft). The bias error for all three flights was 15 m (49 ft). The high-frequency MODILS elevation error had a 0.02° standard deviation. The elevation error pattern repeated itself almost exactly for the 12 approaches. In the turn the elevation error was about +0.2°. For the straight-in section of the approach the elevation error was about -0.1°.

The along-track navigation errors, shown in figure 5 for four approaches of one of the flights, include the ground navigation system (TACAN or MODILS) and airborne receiver signal errors, off-nominal atmosphere effects on the altimeter, errors in the radar tracking data, and the basic navigation system

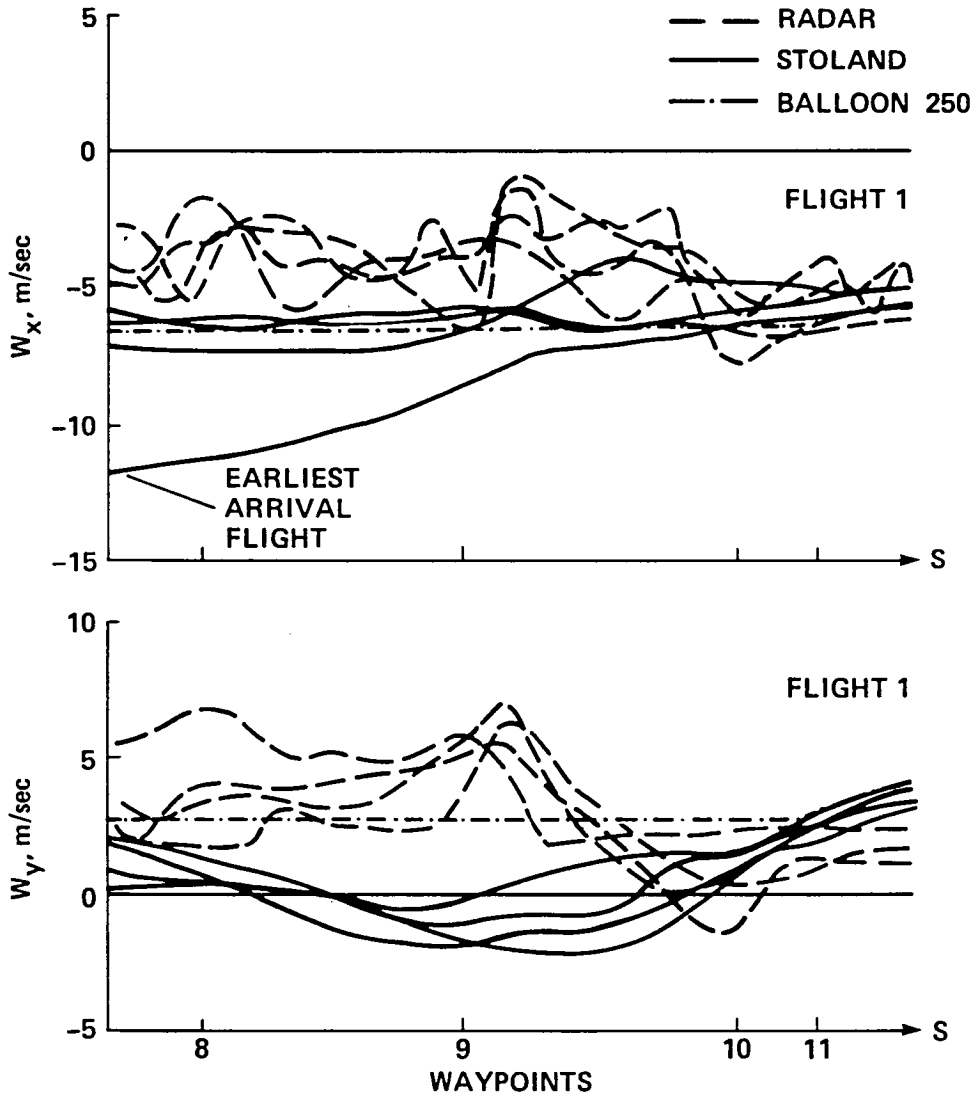

Figure 4.- Comparison of STOLAND estimated winds with balloon and radar-derived wind measurements.

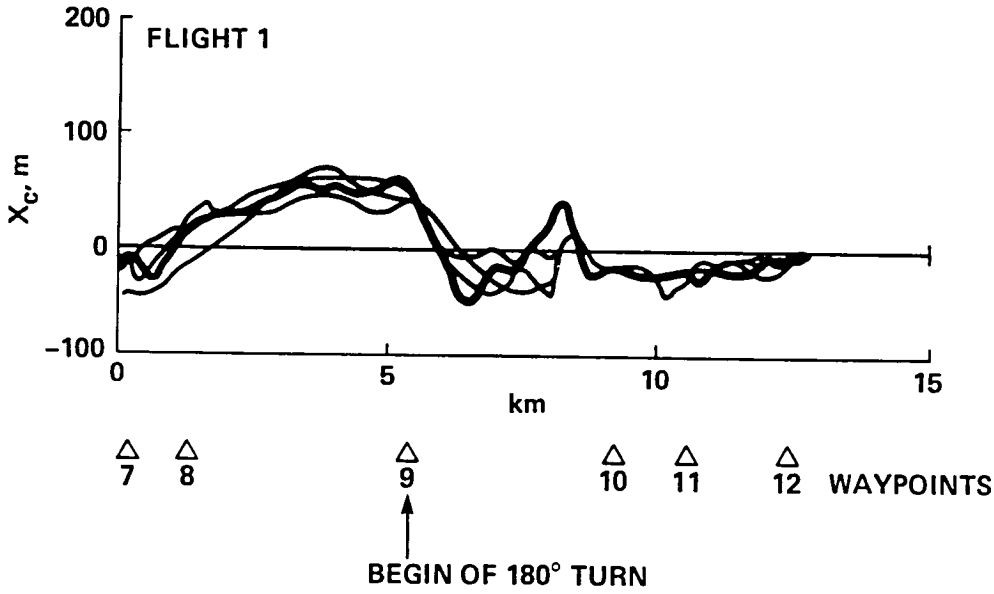

Figure 5.- Alongtrack navigation errors.

errors resulting from software/hardware mechanization. In these figures, the abscissa is the distance (S) along the track. For orientation, the waypoints are labeled on the figures. Waypoints 9 and 10 describe the final turn, and waypoint 12 is the final waypoint for time-of-arrival control. Data for a typical approach are shown as a heavy line. All other approach data are shown as light lines, to give an overview of the variation of the data among approaches. Along-track navigation errors are positive if the estimated position is ahead of the actual (radar-derived) position. The derivation of the equations for the navigation error calculations is given in appendix B of reference 3.

The along-track navigation errors contribute to time-of-arrival errors at the final waypoint. As expected, the navigation errors had different characteristics on different days (not shown), since the TACAN bias errors on different days distorted the measured flightpaths differently. The MODILS portion of the flightpath was similar since MODILS errors were small and did not change from day to day. For the approaches shown, the navigation error tended to be positive between waypoints 7 and 9, which means that the 4D-RNAV system underestimated the distance the aircraft had to go. This in turn would result in a lower V_c and a late arrival at the final waypoint.

This point can better be illustrated by looking at the along-track guidance errors shown in figure 6 for the same four approaches. Along-track guidance errors are positive if the desired aircraft position is ahead of the actual position. The characteristics of the curves are different even for the four approaches, because the time-of-arrival calculations are based on wind estimates whose values at the starting waypoint are different.

There is one common trend in the guidance errors for all four approaches. The actual position tended to fall behind the desired position in the first half of the turn, and tended to catch up in the second half. This was because the reference aircraft position calculations are correct for the endpoints only and do not appropriately account for the winds and deceleration during the turn. Given that the wind measurement is correct, the speeds and arrival times will be correct at the endpoints, but not at intermediate points. The situation could have been improved by defining additional waypoints around the turn.

In figure 7, the along-track guidance errors for the two long approaches and for the five additional approaches that did not continue to waypoint 12, are shown. To produce a plot that is correlated by waypoints, the abscissa has been arbitrarily scaled in waypoint numbers rather than distance along the track. Graphs are labeled in the time sequence they were flown. The following observations can be made. For the first straight constant altitude section (waypoints 1-3) the guidance errors remain small. In the descending turn (waypoints 3, 4) the navigation errors and wind changes with altitude caused the wind estimates to change and errors began to build up. These errors were then reduced as the flight continued. The curves labeled 3-1 and 3-2 and 5-1 and 5-2 are pairs of approaches that were flown sequentially. It will be noticed that both members of each pair show similar errors since the winds and navigation errors had not changed much between sequential approaches.

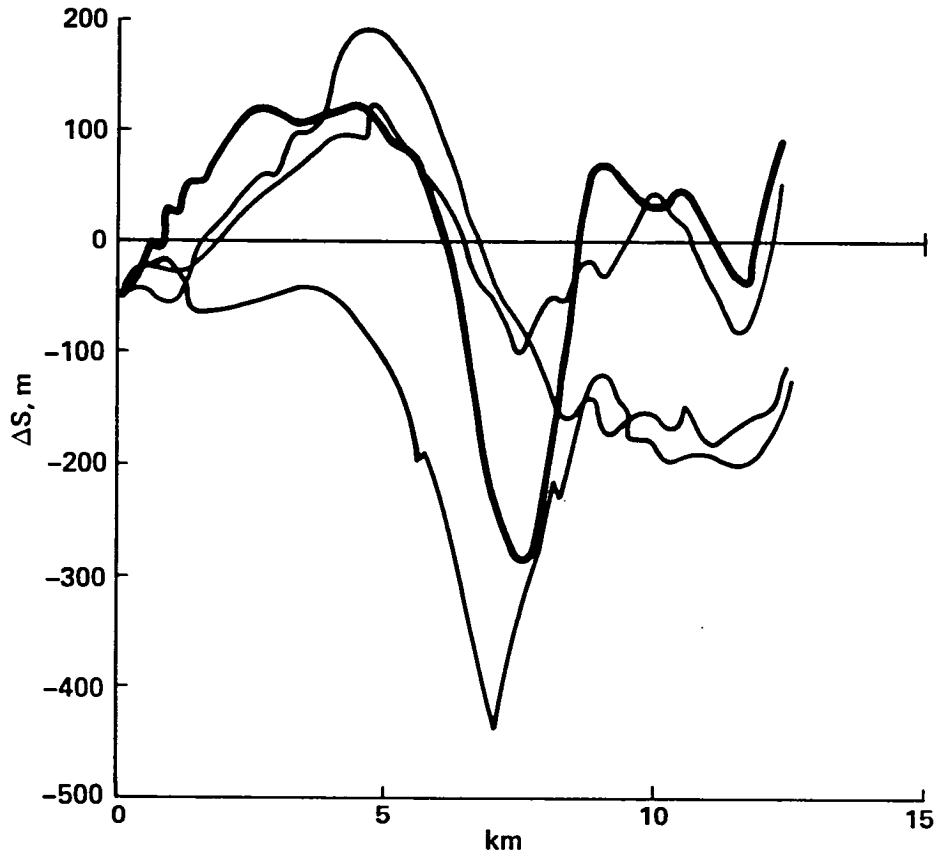

Figure 6.- Alongtrack guidance errors.

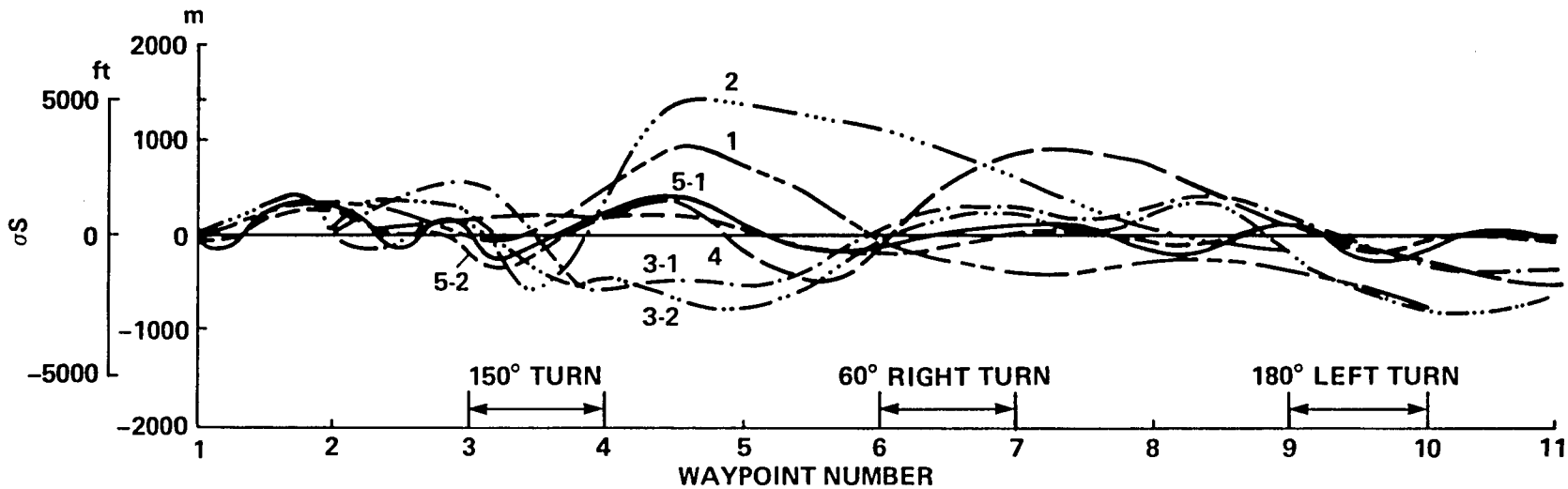

Figure 7.- Alongtrack guidance errors for the long flightpath.

Figure 8 is a histogram of the time-of-arrival errors at waypoint 12 for the 12 approaches (10 short, 2 long) that were continued to waypoint 12. For these tests, the mean time-of-arrival error was -1.02 sec, with a standard deviation of ±1.85 sec.

Fast-Time Simulation: Constant and 4D-RNAV Mechanization

The fast-time simulation was used to look at approaches starting from both waypoint 1 and waypoint 7. Depending on the wind measured, the computed nominal flight times varied. For the set of winds used, the average calculated flight time for the full flightpath was 794 sec, with a standard deviation of 59 sec. For the flight beginning at waypoint 7, the average computed flight time was 233 sec, with a 7-sec standard deviation. The complete set of means and standard deviation of the important statistical quantities are tabulated against the system parameters and other test conditions in appendix F.

The time-of-arrival errors for the constant-wind 4D-RNAV technique are summarized in figure 9. Shown is a plot on normal probability graph paper of the cumulative distributions of time-of-arrival error (T_e) for the approaches starting from waypoint 1 and waypoint 7. The values of the mean time-of-arrival error are similar. Neither curve is straight, indicating that the distributions are not normal. The tails of the distribution curves are markedly longer than those for normal distributions with the same variance. The curve for the longer flightpath shows that 2.3% of the flights arrived more than 3 sec early and 0.6% arrived more than 3 sec late. The equivalent figures for the short flightpath are 0.6% and 0.4%. The differences between the two sets of numbers are due to the error contribution resulting from descending from 2408 m (7900 ft) to 567 m (1860 ft) through unknown and changing winds, the shorter approach having the smaller time-of-arrival errors. To determine if speed-limiting (which occurred because of the maximum and minimum allowable speeds specified by the 4D-RNAV system for each point of the reference flightpath) was responsible for the tails on the distribution curves, 20 early arrivals ($10 > T_e > 1.5$ sec), 20 late arrivals ($-4 < T_e < -1.5$ sec), and 20 on-time arrivals were selected from 770 flights that were started from waypoint 1 for detailed analysis. For the on-time arrivals, speed-limiting occurred much less frequently than in either of the other two cases. Surprisingly, in many of the early-arrival cases there is considerable maximum speed limiting early in the flight. In other words, the system functioned as if late, an error which could not be fully corrected by later commanding the minimum allowable speed. However, for the four extremely early arrivals tabulated in figure 9, the maximum speed was never commanded; the minimum speed was commanded for at least 378 sec along the path.

Comparison of Flight-Test and Fast-Time Simulation Results

The cumulative time-of-arrival comparison of flight data with fast-time simulation data is also shown in figure 9. It can be seen that the simulation and flight data are offset from each other. The 50% point of the flight data cumulative distribution curve is at -1.7 sec (50% of the data points above and

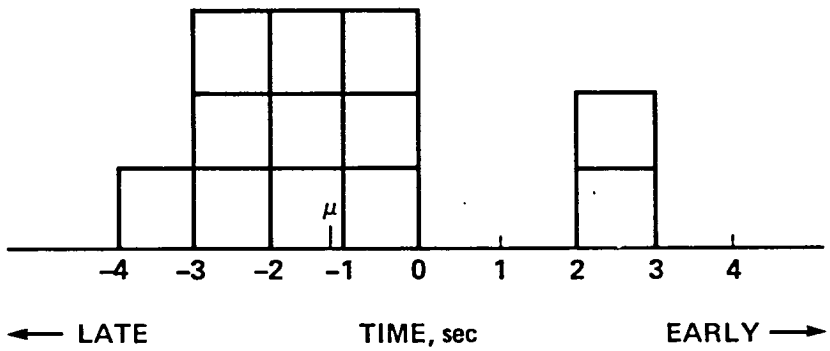

Figure 8.- Arrival-time error histogram.

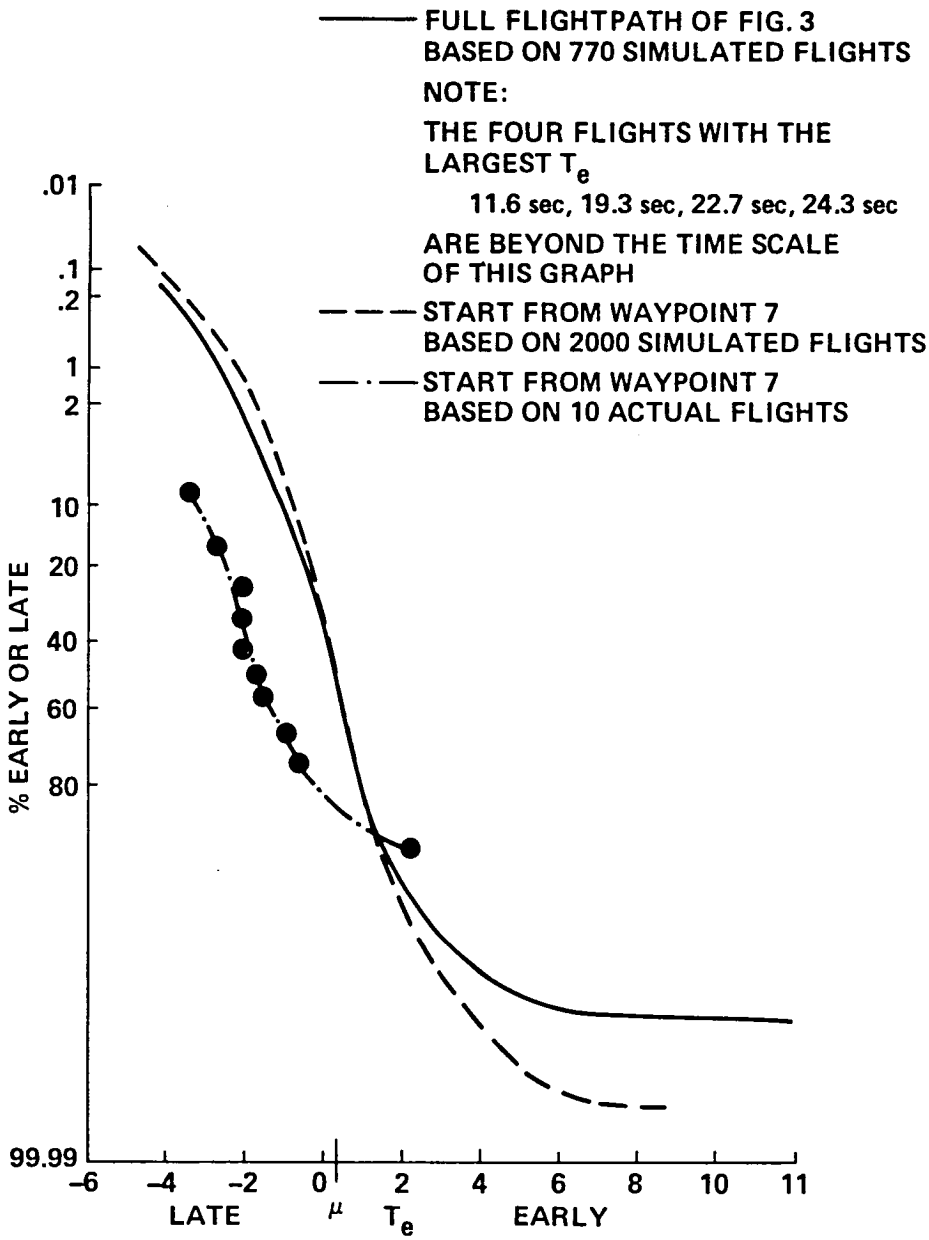

Figure 9.- Empirical cumulative distribution of time-of-arrival error.

50% below). However, the 50% point for the simulation data is at 0.3 sec early. The tendency for the flight data to be late is explained as follows. First, as stated in appendix A there were minor errors in the flight program; those errors caused the aircraft to be late by an average of 1 sec. Second, for the eight approaches of Flights 2 and 3 the TACAN DME error was such that the aircraft flew on the outside of the desired path. As a result, the aircraft flew a longer path than expected by the system, and was always late. For the first flight the TACAN DME error was such that the aircraft flew slightly on the inside of the desired path, resulting in an arrival that was about 2 sec early.

The second approach of Flight 1 was subjected to a special analysis because it arrived 2.8 sec early, which was the largest early arrival error of the 12 approaches. In this case the wind component along the x-axis estimated at waypoint 1 (12 m/sec (39 ft/sec)) was more than twice the value of the actual wind (5 m/sec (16 ft/sec)). This caused a calculated flight time of 248 sec, which was at least 10 sec longer than for the other three approaches, where the wind estimate was closer to the actual wind. To cope with this additional 10 sec, the commanded aircraft speed should have been reduced below the nominal speed. To make matters worse, in the beginning of the flight the aircraft *seemed* to be late, since the actual wind was smaller than the estimated one. To compensate for this, the aircraft speed was increased. After the turn (waypoints 9, 10) the already developed error could not be fully made up by speed reduction, and the 2.8-sec early arrival results.

Comparison of Constant-Wind and Variable-Wind 4D-RNAV Techniques

If the 4D-RNAV-assumed wind and the wind estimates along the path are correct, the aircraft will follow the nominal speed profile, no speed-limiting will occur, and small errors will be corrected in the linear range of the system. The initial assumption of a constant-wind profile, based on the estimated wind at the start of the flightpath, provided a poor estimate of the complete wind profile which resulted in large time-of-arrival errors. Even when the system used maximum allowable effort to correct the error, that effort was insufficient, and, therefore, the system ended up with a relatively large error.

Using the fast-time simulation to investigate the benefits of the variable-wind technique, it was found that the time-of-arrival errors for the variable-wind technique were reduced in 79% of the flights below that of the constant-wind technique, with a substantial reduction in the larger errors. For the remaining 21% of the flight the errors, which were already small, increased slightly. Also, the deviation from the nominal-speed profile was reduced by 35% and the standard deviation of the time-of-arrival error was reduced from 2.0 sec to 0.4 sec.

The cumulative distribution of the time-of-arrival errors for these simulated flights is shown in figure 10. Although the system's overall performance still fails to be normally distributed, figure 10 shows that the large errors in time of arrival have been considerably reduced using interpolated wind

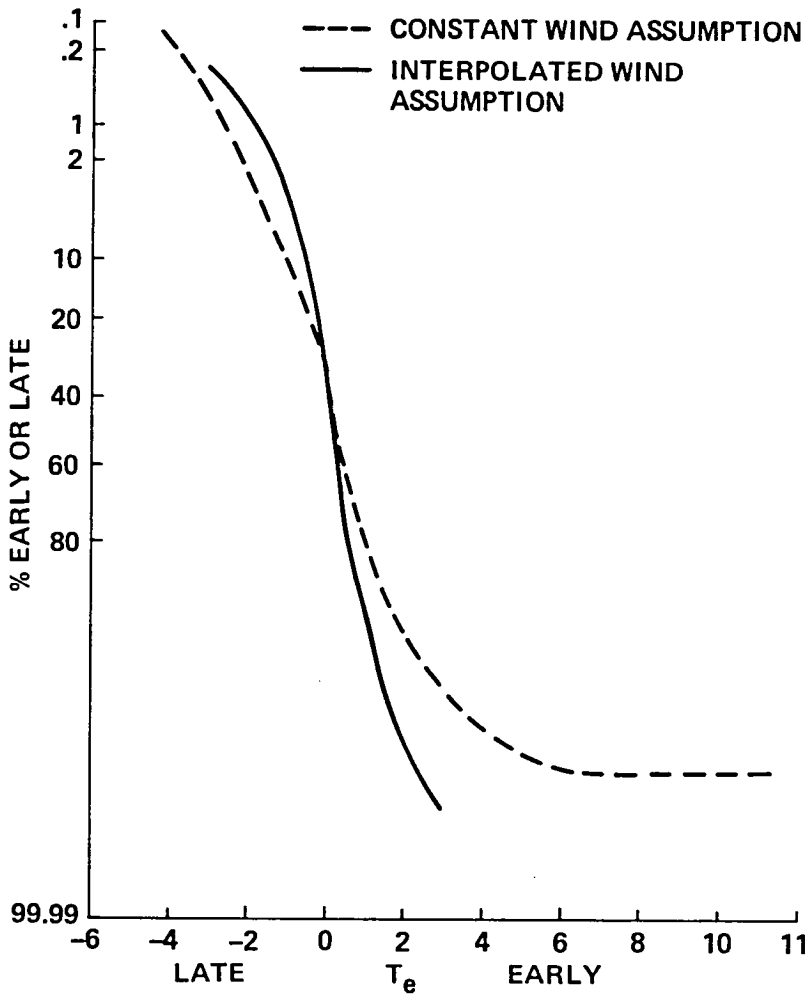

Figure 10.- Empirical cumulative probability distribution of time-of-arrival error.

calculations. From the foregoing discussion it can be seen that there is a definite advantage in using the interpolated wind methods for time-of-arrival calculations. For the infrequent case that the ground wind at the airport may not be available, the performance of the interpolated wind method was investigated with the estimated ground wind set to zero. The standard deviation of time-of-arrival errors was 0.5 sec for the variable-wind 4D-RNAV technique, 0.8 for the same system with zero ground wind assumption, and 0.9 for the constant-wind technique. This shows that the interpolated wind method, which uses the reported ground wind, is better than the same method with a zero ground wind input. However, the latter method has been shown to be statistically as good as the constant-wind 4D-RNAV technique. Hence, the variable-wind technique is preferable, even if there are times when the ground-wind data are not available. These conclusions have been confirmed to be statistically significant by Student's t-tests at the 1% confidence level where the time-of-arrivals of the corresponding flights were compared in pairs.

CONCLUSIONS AND RECOMMENDATIONS

This study has been concerned with 4D RNAV for jet STOL aircraft, using the AWJSRA as a representative aircraft type. Flight tests were used to verify simulation results, to test the automatic configuration control, and to get operational experience. Fast-time simulation was used to determine the overall performance of the time-of-arrival control system for a particular flightpath, radio navigation aid location, and 4D-RNAV speed limits.

The following conclusions were reached from this simulation and flight study:

1. The accuracy of the 4D-RNAV wind estimates is dependent on the accuracy of the ground navigation errors. For these tests, the error in the wind estimate was as high as 10 knots when TACAN was used. When MLS was used as the primary navigation source, the error was reduced to less than 2 knots.

2. The navigation errors and errors in the wind estimates strongly affect the time-of-arrival error. Neither the navigation errors nor wind errors are repeatable from day to day, and therefore the time-of-arrival errors will be different.

3. In the 4D-RNAV mechanization evaluated, the reference aircraft position calculations were correct only at the waypoints and did not appropriately account for winds and for the effect of deceleration during the turn. The situation can be improved by defining additional waypoints around the turn.

4. The results of the flight test combined with the fast-time simulation demonstrated that the constant-wind 4D-RNAV technique achieved a time-of-arrival error standard deviation of less than 2 sec. Only 2.3% of the flights arrive more than 3 sec early and 0.6% arrive more than 3 sec late.

5. If speed-limiting occurs due to the restrictive operating range of aircraft speeds, large time-of-arrival errors can occur. In these tests errors of greater than ±4 sec occurred for 1.3% of all approaches.

6. Based on results of the fast-time simulation, the variable-wind 4D-RNAV technique resulted in a significant reduction of time-of-arrival errors over the constant-wind 4D-RNAV technique. The standard deviation was reduced from 2 sec to 0.4 sec and errors greater than ±4 sec were reduced from 1.3% of all approaches to only 0.4% of all approaches.

APPENDIX A

COMPARISON OF FAST-TIME AND REAL-TIME SIMULATION

The piloted real-time simulation includes full simulator cockpit instrumentation and uses software identical with the flight software. In fact, the simulator is used to check out flight software. To verify the fast-time simulation, nine pairs of flights with nine different wind profiles were flown on the real-time simulation and on the fast-time simulation on identical flightpaths. The real-time simulation always arrived later, by an average of 1 sec, than the corresponding fast-time simulation. Time histories of ΔS were plotted. They agreed in trend but not completely in magnitude. To study these minor differences, the time-of-arrival tables for the two simulations were compared. The comparison showed that the fast-time simulation calculated flight times for the 600-sec path that were between 7 and 10 sec longer than the real-time simulation. This was traced to several improvements in the arrival-time calculations that had been made in the fast-time simulation, but not implemented in the real-time simulation. When these improvements were incorporated in the flight program, the time-table calculation differences were reduced to 5 sec maximum, or less than 1%. The remaining differences resulted from round-down truncation errors in the integration, using the fixed-point 1819 computer. The original 7-10 sec underestimation of the flight time, which the real-time system tried to adhere to in spite of later wind shifts, had to be made up by speed control, which explains the tendency for the real-time system to show time-of-arrival error that was positive. In summary it can be said that the fast-time system is a good (but somewhat improved) representation of the flight program that was used in the real-time simulation.

APPENDIX B

THE MASTER TABLE OF FAST-TIME SIMULATION RESULTS

The master table is a summary of the simulation results concerned with time-of-arrival control. First, the parameters will be defined that have been varied during the tests. Then the table will be presented followed by brief comments on the significance of the tests.

1. Feedback (Fb)

$$V_c = V_{nom} + K_f \Delta S \left|\frac{T_{ref}}{T}\right|_{\leq 1}$$

yes → $K_f = 0.04$ where T = time to go

no → $K_f = 0$

2. T_{ref} = time to go at which maximum constant gain is used.

3. Smooth

yes = with arrival time estimate smoothing

no = without arrival time estimate smoothing

(See ref. 18 for definition of smoothing.)

4. Update = time interval in seconds at which time of arrivals at the waypoints are recalculated based on the latest wind information.

5. Wind calculations

5.1 Constant (C): calculates arrival time at each update interval as if the wind would remain constant at the presently measured wind for the remainder of the flight.

5.2 Interpolate (I): calculates arrival times at each update interval as if the wind would vary linearly with altitude from the presently measured wind to the actual ground wind.

5.3 Exact (E): calculates arrival times from the known wind profile.

Flight set	Systems parameters 1 Fb	2 T_{ref} (sec)	3 Smooth	4 Update	5 Wind	Environmental conditions 6 Wind	TACAN DME errors	TACAN A_z (°) errors	Flight-path	No. of flights	Statistical measures of test outcomes: Phantom position error $\lvert\Delta S\rvert$ ft μ	σ	Deviation from nominal speed profile $\lvert V_{com} - V_{nom_L}\rvert$ μ	σ	Throttle activity $\sigma\left(\frac{V_{com} - V_{com_L}}{\Delta t}\right)$ μ	σ	Time of arrival error T_e (sec) μ	σ
1	no	200	yes	10	E	1-27				27	73	27	0.01	0.002	0.30	0.01	0.7	0.3
2	no	200	yes	10	I	1-27	0	0	Fig. 3	27	1754	1060	0.02	0.006	0.32	0.01	-6.0	11.7
3	no	200	yes	10	C	1-27				27	2884	1708	0.03	0.045	0.33	0.02	-11.2	17.7
4	yes	200	yes	10	E	1-27				27	17	5	0.43	0.11	0.30	0.01	0.0	0.1
5	yes	200	yes	10	E	1-27	0	0	Fig. 3	27	299	150	5.30	2.42	0.32	0.02	0.0	0.5
6	yes	200	yes	10	C	1-27				27	544	453	7.59	3.76	0.33	0.04	0.5	0.8
7	yes	200	yes	20	C	1-27				27	537	449	7.57	3.76	0.34	0.04	0.5	0.9
8	yes	200	yes	20	I	1-27	0	0	Fig. 3	27	293	141	5.26	2.41	0.33	0.02	0.0	0.5
9	yes	200	no	10	C	1-27	0	0	Fig. 3	27	548	456	7.60	3.76	0.52	0.12	0.4	0.8
10	yes	200	no	10	I	1-27				27	298	150	5.40	2.45	0.47	0.08	0.1	0.4
11	yes	50	yes	10	I	1-27				27	736	393	4.01	1.98	0.32	0.02	0.0	0.5
12	yes	100	yes	10	I	1-27				27	485	248	4.70	2.20	0.32	0.02	0.0	0.5
13	yes	300	yes	10	I	1-27	0	0	Fig. 3	27	224	116	5.53	2.49	0.33	0.02	0.0	0.4
14	yes	400	yes	10	I	1-27				27	188	100	5.65	2.51	0.33	0.02	0.0	0.4
15	yes	1000	yes	10	I	1-27				27	153	83	5.77	2.52	0.34	0.03	0.0	0.4
16	yes	200	yes	60	C	1-27				27	502	426	7.51	3.75	0.34	0.04	0.5	1.0
17	yes	200	yes	60	T	1-27				27	269	136	5.11	2.37	0.34	0.03	0.0	0.5
18	yes	200	yes	1000	C	1-27	0	0	Fig. 3	27	390	241	7.69	3.35	0.40	0.09	2.3	11.8
19	yes	200	yes	1000	I	1-27				27	210	116	4.67	2.39	0.37	0.07	-0.07	2.3
20	yes	200	yes	1000	E	1-27	0	0	Fig. 3	27	17	5	0.43	0.11	0.30	0.01	0.0	0.1
21	yes	200	yes	20	I	7				50	348/251	127	6.9/5.3	2.27	0.38/0.33	0.05	0.0/0.0	0.7
22	yes	200	yes	20	I	11				50	854/676	276	11.5/9.6	2.28	0.40/0.36	0.04	1.3/1.0	0.9
23	yes	200	yes	20	I	14	0	0	Fig. 3	50	389/335	160	7.6/6.9	2.49	0.36/0.31	0.05	1.3/0.9	1.2
24	yes	200	yes	20	I	19				50	297/259	125	5.3/2.5	2.01	0.37/0.32	0.06	-0.8/-0.8	0.9
25	yes	200	yes	20	I	21				50	549/428	191	8.6/6.5	2.44	0.38/0.32	0.05	0.6/0.4	0.9
26	yes	200	yes	10	I	1-27	0	0	Fig. 3	27	322	159	5.265	2.16	0.33	0.02	0.0	0.3
27	yes	200	yes	10	C	1-27				27	720	593	8.45	3.59	0.35	0.04	0.3	0.5
28	yes	204.7	yes	20	C	RD**	random bias errors see app. F	random bias errors see app. F	" WP7-12 only	2000	339	382	7.20	4.12	0.54	0.14	0.1	1.0
29	yes	204.7	yes	20	C	RD			Fig. 3	422	876	901	10.97	4.78	0.39	0.08	0.2	1.8
30	yes	204.7	yes	20	C	RD				348	967	1078	11.17	4.99	0.39	0.09	0.3	2.1
31	yes	204.7	yes	20	C	RD	0	0	Fig. 3	302	794	1002	9.26	4.88	0.33	0.05	0.3	2.0
32	yes	204.7	yes	20	C	RD	1000	2.0	Fig. 3	305	1053	1133	11.81	4.36	0.53	0.04	3.4	3.6
33	yes	204.7	yes	20	I	RD	1000	2.0	Fig. 3	167	631	318	9.32	3.24	0.51	0.02	2.0	1.0
34	yes	204.7	yes	20	I	RD	-1000	-2.0	Fig. 3	192	526	282	10.00	3.17	0.37	0.04	-0.8	0.7
35	yes	204.7	yes	20	I*	RD	0	0	Fig. 3	111	438	324	6.76	3.53	0.33	0.03	-0.3	0.8
36	yes	204.7	yes	20	I	RD	random bias errors	random bias errors	Fig. 3	232	464	283	7.56	3.12	0.38	0.07	0.0	0.8
37	yes	204.7	yes	20	I	RD				131	493	319	8.00	3.60	0.38	0.08	0.0	0.7
38	yes	204.7	yes	20	I	RD	0	0	Fig. 3	170	271	391	6.00	3.2	0.32	0.03	0.0	0.4

*With zero ground-wind assumption.

**RD = random wind profile (see appendix E).

Comments referring to flight sets	Comments to master table
1, 2, 3	Performance of system without error feedback shows that interpolated system would have less correcting to do than constant-wind system.
4, 5, 6	Same as 1-3 except with feedback correction. Shows how feedback reduces errors at small cost of throttle activity. Shows interpolated wind system better than constant.
9-5, 10-6	Compare 9 with 5 and 10 with 6 — Smoothing primarily reduces throttle activity.
11, 5, 12, 13, 14, 15	See also 5. Gain scheduling primarily reduces deviations from the nominal speed profile without affecting time-of-arrival errors.
6, 7, 16, 18; 5, 8, 17, 19	Compare Flight Sets 6-7-16-18 for variation in time-of-arrival table updating for constant-wind assumption and 5-8-17-19 for interpolated wind. Arrival-time errors get worse with less updates. Constant system is more sensitive to longer update times. Faster update reduces throttle activity somewhat.
4,20	Compare to 4 — Updating is irrelevant when exact wind is known.
21, 22, 23, 24, 25	Add 8 fps low pass filtered random wind T = 900 sec to different known wind profiles to determine additional errors due to randomness of the wind with time. Numbers behind the slash are for the given wind without additional random wind component. TOA errors become larger and the throttle activity goes up by 13%.
26-5; 27-6	Exact wind at the aircraft position used for TOA calculations at each update point. Compare 26-5 and 27-6. Slight improvement in time-of-arrival error with exact wind.
28	WP 7-12 only — Wind from random wind profile model.
29, 30	Full flightpath; wind from random wind profile model; combine flights to get overall statistical performance.
31, 32	Comparing 31-32 shows effect of specific navigation bias error.
32, 33	Flights same as first 167 in Flight 32 — See improvement due to interpolation of wind.
33, 34	Compare 33-34 for biasing effect of specific navigation error.
35	Zero ground wind assumption (35) with interpolation is better than constant wind model (31).

Comments referring to flight sets	Comments to master table (Concluded)
36, 37	Combine and compare to 29 + 30. Time-of-arrival error is reduced.
35, 36	Compare with 35 and 31. It is good to know ground wind but if not available assume ground wind is as good as constant assumption.

APPENDIX C

AIRCRAFT SPEED AND SAFETY LIMITS

Aircraft configuration-dependent speed/safety limits are computed in addition to the 4D-RNAV specified speed limits. The speed/safety limits will always override any 4D speed limits in cases where these 4D limits fall outside the designated safe limits. The maximum speed limit is determined by the structural flap placard speed. The minimum speed is based on the maneuver margin, where L is a measure of the aerodynamic lift available, provided the thrust is not changed:

$$\frac{n = L \text{ max} - L}{W} \text{ (g)}$$

With flaps up, a maneuver margin of 0.69 g was selected, which is equivalent to the well-known minimum conventional takeoff and landing approach speed, 1.3 V_{stall}. When flaps are extended, the powered-lift augments aerodynamic lift, and the aerodynamic maneuver margin is lowered to 0.4 g, beyond 30° flap deflection. Between 5.6° and 30° of flaps the maneuver margin smoothly decreases from 0.69 g to 0.4 g. As bank angle protection prior to glide-slope capture, 3 knots are added to the minimum speed computed. When the nozzles are deployed a minimum speed related to the landing airspeed is computed.

In the flightpath design it is desirable that the 4D-RNAV limits agree as closely as possible with the aircraft speed limits. If the aircraft limits are much larger than the 4D limits, the error correcting capability of the system is not fully used. If the aircraft limits are much smaller than the 4D limits, the 4D system, based on the 4D speed limits, calculates maximum and minimum possible times of arrival that are not realistic. Hence, the system may indicate to the pilot that it is capable of correcting an existing error, when indeed it is not.

APPENDIX D

THE NAVAID TRANSITIONING CIRCUIT

The NAVAID transitioning circuit is described here, because it is not described in other STOLAND documentation, and because it affects the reported results. When the aircraft navigation transitioned from TACAN to MODILS, or from dead reckoning to a NAVAID, relatively large step changes in the input to the navigation filters were noted. These changes resulted in large transients in both speed and position estimates, which, when the aircraft is in 4D RNAV, can result in undesirable aircraft motions. To minimize these transients and to reduce the aircraft motions, a NAVAID transitioning circuit has been added to the navigation system (see fig. 11). The transitioning circuit works as follows. At transition a value X is calculated where X is the difference between the new raw (unfiltered) position estimate, X_R, and the old filtered position estimate, $\hat{X}_I$.

$$\Delta X = X_R - \hat{X}_I$$

If the difference X is smaller than 2 n. mi. the filtered position estimate, X_I, is reset to the new raw position estimate

$$\hat{X}_I = X_R$$

The position estimate, $\hat{X}$, which is used by the guidance system, is calculated as

$$\hat{X} = \hat{X}_I - X$$

At the moment of transition, X is equal to the old position estimate

$$\hat{X} = \hat{X}_I - \Delta X = X_R - (X_R - \hat{X}_I) = \hat{X}_I$$

and there is no transient disturbance in the estimated position. At the same time, $X_e = X_R - \hat{X}_I = 0$ and there is no transient in the velocity estimate. The value ΔX is now reduced to zero at a rate of 12.2 m/sec (40 ft/sec) so that the guidance system finally depends fully on the new navigation source. This process is slow enough so that the resultant aircraft motions are not noticeable to the pilot.

Other sources of navigation errors are biases on the aircraft gyros and accelerometers after the turn to final. Hence, when transitioning from TACAN to MODILS, the complementary filter gains are changed from the low values for TACAN navigation to high values for MODILS in order to quickly integrate out bias errors in the acceleration inputs to the complementary filters, which are introduced by the roll and heading gyros. If the gains were changed suddenly, however, large filter transients might occur if the TACAN bias errors were

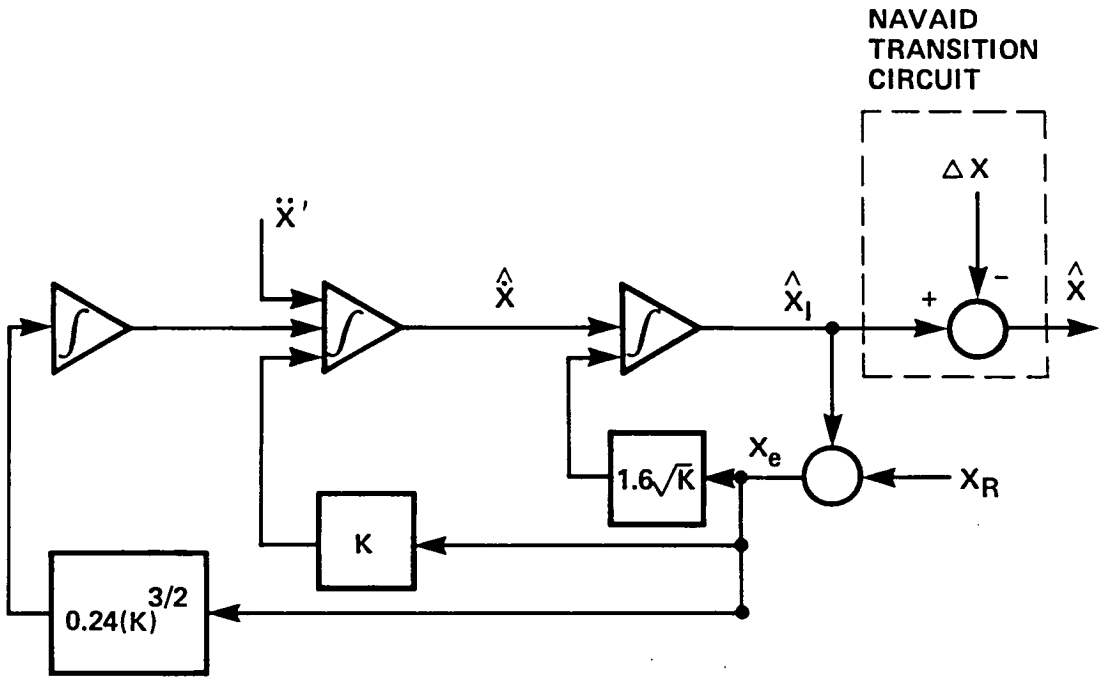

Figure 11.- Complementary filter.

large. Therefore, the complementary filter gains were linearly reduced with time from the TACAN gains to the constant MODILS gains.

One further difference between the navigation filter described in reference 23 and the new navigation filter is the calculation of the wind vector. In the previous filter it was assumed that the aircraft heading was in the direction of the airspeed vector, which is correct for straight and level flight without sideslip. For coordinated turns, the relation between the aircraft heading and the velocity vector is shown in figure 12. The airplane's heading is into the turn by an angle $\Delta\psi$ where

$$\Delta\psi \cong \theta \tan \phi$$

This angle is therefore subtracted from the heading as an approximation of the track angle, which then is used in the wind calculation to compute airspeed components along the x and y axes of the runway oriented coordinate system.

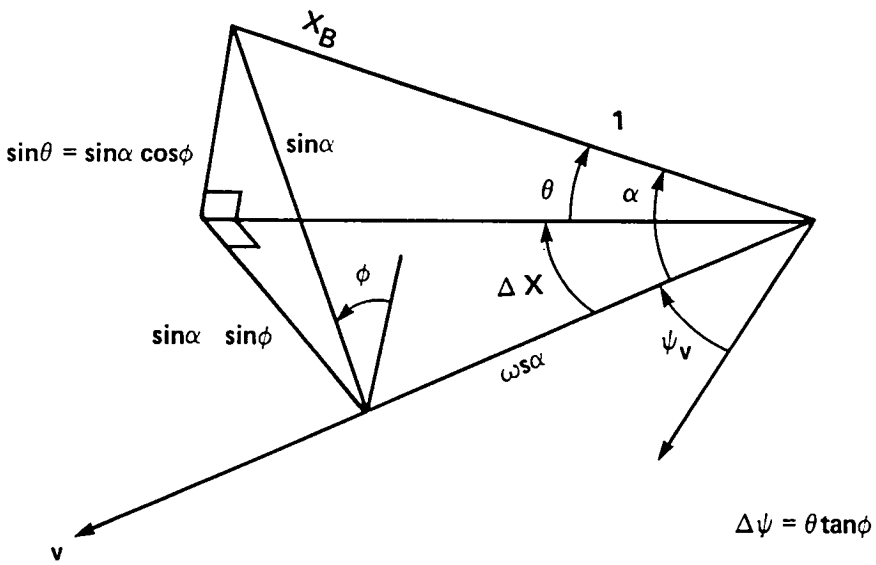

Figure 12.- Angle between heading and velocity vector in a coordinated turn.

APPENDIX E

THE RANDOM WIND PROFILE MODEL

The random-wind-profile model was generated from statistical examination of the sample-wind profiles, obtained from the Oakland Weather Station and by combining this information with FAA information about the wind direction and magnitude for automatic landing studies. For the ground-wind direction ψ we select randomly from a truncated normal distribution such that two-thirds of the winds have a headwind component $90° \leq \psi \leq 270°$, where the peak value is a pure headwind component along the landing direction ($\psi = 180°$). The ground-wind magnitude, W_g, is chosen from a normal distribution so that the 3-sigma headwind is 25 knots, sidewind 15 knots, and tailwind 10 knots.

$$\text{Sigma} = 1/3(15 - 7.5 \cos \psi + 2.5 \cos^2 \psi) \quad \text{(knots)}$$

$$Wg = |N(0, \text{Sigma})| \quad \text{(knots)}$$

The winds at altitude are determined by the following calculations in 305-m (1000-ft) intervals for $h = 1000, \ldots, 9000$

$$W_h = W_{h-1000} + (1.1 + 1.3e^{(1000-h)/2000}) + 3N(0., 1.) \quad \text{(knots)}$$

Thus the wind tends to grow with altitude, first rapidly then less rapidly. The wind direction is selected from

$$Az_h = Az_{h-1000} + A_s \cdot N(0., 1)|_{\text{Limit } 3\sigma} \quad \text{(deg)}$$

where

$$A_s = |12. + 17.5e^{(1000-h)/1000}| \quad \text{(deg)}$$

and the sign of the A_s is selected from a two-valued probability distribution, which is a probability of 0.78 that the wind angle changes in the same direction as the wind angle of the last lower altitude and a probability of 0.22 that the wind angle changes in the opposite direction.

APPENDIX F

TACAN POSITION AND NAVIGATION ERROR MODEL

Flight data have shown that flying close to a TACAN station presents guidance problems because of the effects of the bias errors on position and groundspeed estimation. For the test flights at Crows Landing, the TACAN station was at one specific location with respect to the runway. In general, the relative location changes from airport to airport. Two questions must therefore be explored: (1) How are the NAVAIDs located? and (2) How does the location of the NAVAID affect path control? Figure 13 shows the positions of TACAN, VOR and VORTAC stations with respect to the runway threshold for 52 airports in California, Nevada, Utah, and Arizona that have radio NAVAIDs on the field. Most lie within 6000 m to either side of the runway. The data have been obtained by scaling the figures in reference 24, using the published runway lengths. The locations have been verified for six cases by plotting the longitude and latitude of the station given in reference 24 on the maps in reference 25. It is clear that an RNAV system must operate successfully for ground NAVAIDs located anywhere within the region occupied in figure 13. For statistical evaluation, the TACAN azimuth has a normal distribution within a mean bias of zero and a standard deviation of

$$\sigma_{\psi_B} = -0.59°$$

and the TACAN DME has a normal distribution with a mean bias of zero and a standard deviation of

$$\sigma_{DME} = 305 \text{ m } (1000 \text{ ft})$$

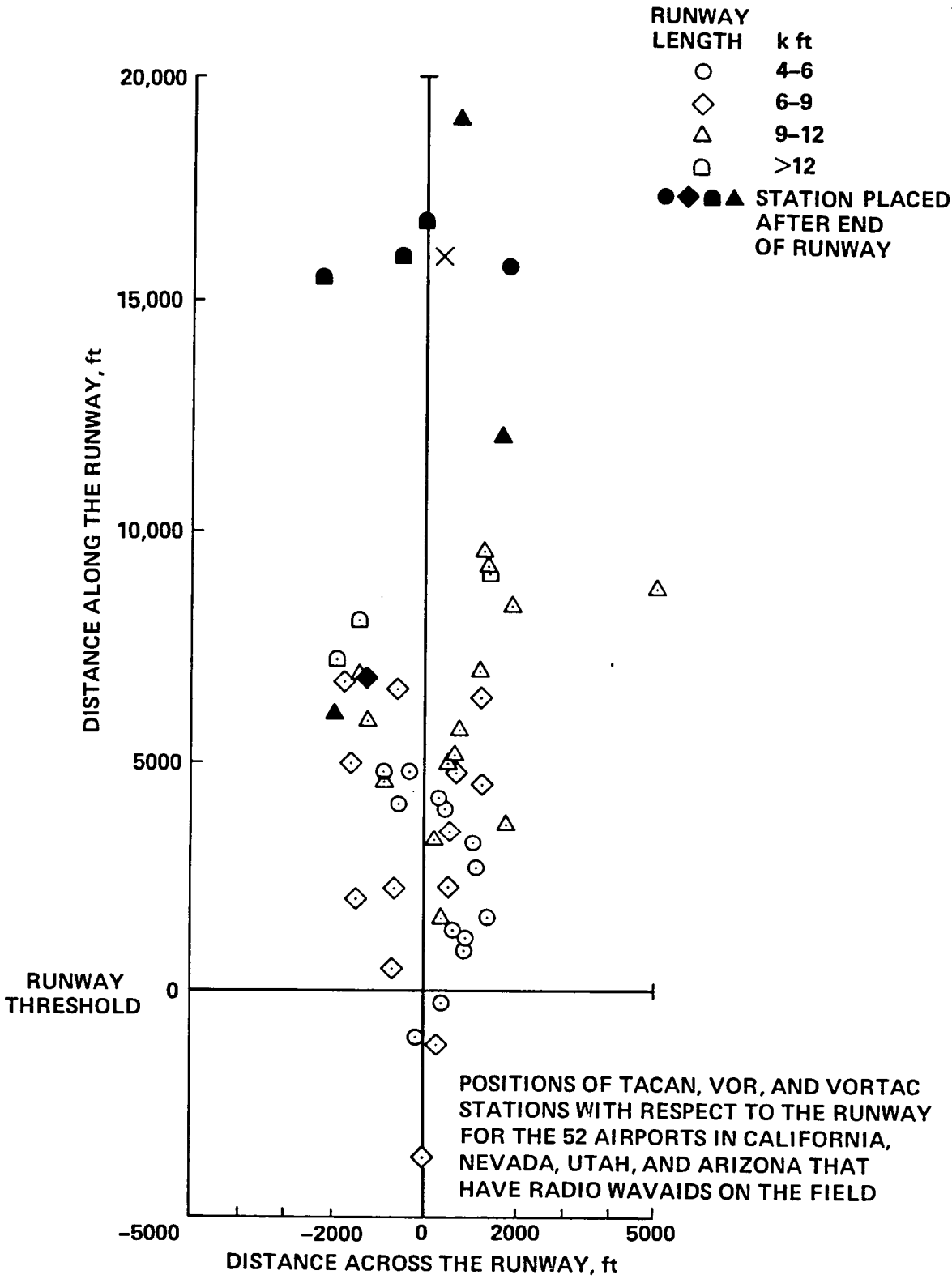

Figure 13.- NAVAID positions.

REFERENCES

1. Civil Aviation Research and Development Policy Study. NASA SP-265, 1971. (Also available as COT TST-10-4.)

2. Application of Area Navigation in the National Airspace System. Report by FAA/RNAV Task Force, FAA Washington, D.C., Apr. 1973.

3. Tobias, Leonard; and O'Brien, Paul: Real-Time Manned Simulation of Advanced Terminal Area Guidance Concepts for Short-Haul Operations. NASA TN D-8499, Aug. 1977.

4. Clark, W. H.; Bolz, E. H.; Solomon, H. L.; and Stephenson, A. R.: Implementation of Area Navigation in the National Airspace System: An Assessment of RNAV Task Force Concepts and Payoffs. Systems Control, Inc., Palo Alto, Calif., FAA-RD-76-196, Jan. 1976.

5. Erwin, R. L., Jr.: Strategic Control of Terminal Area Traffic. Boeing Commercial Airplane Company, Seattle, Washington, in AGARD CP-188, May 1975.

6. Hynes, R. J.; Stevenson, L. E.; and Capen, E. B.: 4D Guidance of STOL Aircraft. AIAA Paper 71-770, Seattle, Wash., 1971.

7. Erzberger, H.; and Pecsvaradi, T.: 4D-RNAV System Design with Application to STOL Air Traffic Control. 13th Joint Automatic Control Conference, Stanford, Calif., Aug. 16-18, 1972.

8. Hemesath, R. B.; Bruckner, J. M. H.; Krippner, R. A.; Meyer, D. H.; and Murphy, J. W.: Three and Four Dimensional Air Navigation Study. FAA-RD-74-150, 1974.

9. Nagarajan, N.: Approach to a Four Dimensional Guidance Problem Near Terminal Areas. International Journal of Control, vol. 20, Aug. 1974.

10. Erzberger, H.; and Menga, G.: Time Controlled Descent Guidance in Uncertain Winds. AIAA Paper 75-1078, Boston, Mass., 1975.

11. Foudriat, E. C.: A General Algorithm for Relating Ground Trajectory Distance, Elapsed Flight Time, and Aircraft Airspeed and its Application to 4D Guidance. NASA TN D-7876, 1975.

12. Nagarajan, N.: Four Dimensional Guidance Problem with Control Delays — In Air Traffic Control Automation. Journal of Aircraft, vol. 13, Aug. 1976, pp. 559-564.

13. Lax, F. M.: Design and Simulation of a Descent Controller for Strategic Four Dimensional Aircraft Navigation. M.S. Thesis. Massachusetts Inst. of Techn., Cambridge.

14. Modlinger, A.: Mission Management in the Airport Vicinity — Digital Flight Control for Terminal Maneuvering Area. DGLR Paper 77-037, Deutsche Gesellschaft Fuer Luft- Und Raumfahrt, Jahrestagung, 10th, Berlin, W. Germany, Sept. 13-15, 1977.

15. Durocher, C. L.: The Effect of Radar Disturbances on Aircraft Runway Arrival Time in a Four Dimensional Navigation Terminal Approach, Digital Avionics Systems Conference. AIAA Paper 77-1512, Los Angeles, Calif., 1977.

16. Neuman, Frank; Warner, David N.; and Moran, Francis J.: A Flight Investigation of a 4D Area Navigation System Concept for STOL Aircraft in the Terminal Area. NASA TM X-73, 1975.

17. Lee, Homer Q.; and Neuman, Frank: 4D Area Navigation System Description and Flight Test Results," NASA TN D-7874, 1975.

18. Neuman, Frank; and Lee, Homer Q.: Flight Experience with Aircraft Time-of-Arrival Control. Journal of Aircraft, vol. 14, no. 2, Feb. 1977, pp. 104-110.

19. Knox, C. E.: Experimental Determination of the Navigation Error of the 4D Navigation, Guidance and Control Systems on the NASA B-737 Airplane. AGARD Guidance and Control Considerations for Low-Altitude and Terminal Area Flight, AGARD CP-240.

20. Cleveland, W. B.; Vosmaske, F.; and Sinclair, S. R. M.: Augmentor Wing Jet STOL Research Aircraft Simulation Model. NASA TM X-62,149, 1972.

21. Neuman, F.; Watson, D.; and Bradbury, Peter: Operational Description of an Experimental Digital Avionics System for STOL Airplanes. NASA TM X-62,448, 1975.

22. Adams, Glen D.: Evaluation of STOL Modular Instrument Landing System (MODILS). Department of Transportation, FAA Rep. FAARD-72-4, 1972.

23. Neuman, Frank; and Warner, David N., Jr.: A STOL Terminal Area Navigation System. NASA TM X-62,348, 1972.

24. Low Altitude Instrument Approach Procedures West United States. Vol. 2. Defense Mapping Agency Aerospace Center, 1978.

25. IFR Supplement Defense Mapping Agency Aerospace Center, 1978.

26. Erzberger, Heinz; and McLean, John D.: Fuel Conservative Guidance System for Powered Lift Aircraft. AIAA Guidance and Control Conference, Aug. 1979, Boulder, Colo.

1. Report No.	2. Government Accession No.	3. Recipient's Catalog No.
NASA TM-81271		

4. Title and Subtitle	5. Report Date
FLIGHT INVESTIGATION OF A FOUR-DIMENSIONAL TERMINAL AREA GUIDANCE SYSTEM FOR STOL AIRCRAFT	March 1981
	6. Performing Organization Code
7. Author(s)	8. Performing Organization Report No.
Frank Neuman and Gordon Hardy	A-8491
	10. Work Unit No.
9. Performing Organization Name and Address	505-34-11
Ames Research Center, NASA Moffett Field, Calif. 94035	11. Contract or Grant No.
	13. Type of Report and Period Covered
12. Sponsoring Agency Name and Address	Technical Memorandum
National Aeronautics and Space Administration Washington, D.C. 20546	14. Sponsoring Agency Code

15. Supplementary Notes

16. Abstract

A series of flight tests and fast-time simulations have been conducted, using the augmentor wing jet STOL research aircraft and the STOLAND 4D-RNAV system to add to the growing data base of 4D-RNAV system performance capabilities. To obtain statistically meaningful data a limited amount of flight data were supplemented by a statistically significant amount of data obtained from fast-time simulation. In this paper, the results of these tests are reported. Included are comparisons of the 4D-RNAV estimated winds with actual winds encountered in flight, as well as data on along-track navigation and guidance errors, and time-of-arrival errors at the final approach waypoint. In addition, a slight improvement of the STOLAND 4D-RNAV system is proposed and demonstrated, using the fast-time simulation.

17. Key Words (Suggested by Author(s))	18. Distribution Statement
4D-RNAV Automatic guidance Terminal area approaches	Unlimited STAR Category - 01

19. Security Classif. (of this report)	20. Security Classif. (of this page)	21. No. of Pages	22. Price*
Unclassified	Unclassified	43	$6.50

*For sale by the National Technical Information Service, Springfield, Virginia 22161